Orthogonal Coding for Millimeter-Wave Imaging using MIMO Dynamic Metasurface Apertures

Vasiliki Skouroliakou, Amir Masoud Molaei, Maria Garcia-Fernandez, Guillermo Alvarez-Narciandi, Okan Yurduseven
Institute of Electronics, Communications and Information Technology (ECIT),
Queen's University Belfast, Belfast,United Kingdom
vskouroliakou01@qub.ac.uk

***Abstract*—The recent advent of dynamic metasurface antennas (DMAs) as a millimeter-wave computational imaging (CI) platform has mitigated the hardware limitations of traditional imaging systems in terms of acquisition time, flexibility and cost. Considering a multiple-input multiple-output (MIMO) system fully realized by DMA panels, real-time simultaneous data acquisition can occur by adopting an orthogonal coded approach which enables concurrent transmission and reception by all DMA panels. The image is then reconstructed in the frequency domain by utilizing a signal decompression step that enables the use of a range migration algorithm (RMA) for the compressed signal received by the DMA panels. In that way, the time for the signal processing layer is also significantly reduced compared to the traditional image reconstruction methods usually applied to DMA-based systems. Simulation results of resolution targets are presented to demonstrate the efficiency of the suggested technique.**

***Index Terms*—Computational imaging (CI), dynamic metasurface apertures (DMAs), millimeter-wave imaging, multiple-input multiple output (MIMO) systems, orthogonal channel coding.**

I. Introduction

A variety of applications, ranging from concealed object detection to through-wall imaging and medical diagnosis, have increasingly relied on millimeter wave (mmWave) technology [1]–[3]. This is mainly because wavelengths in those frequencies have been proven to successfully penetrate common clothing, without being hazardous for human health. Consequently, there is an active research field aiming to construct efficient mmWave systems satisfying the criteria of enough resolution, fast data acquisition time, hardware simplification and, of course, cost minimization.

Computational imaging (CI) systems realized by dynamic metasurface antennas (DMAs) are becoming more and more popular for millimeter-wave applications, since they have been shown to mitigate the hardware limitations of existing mmWave systems, such as those based on synthetic aperture radar (SAR) [4]–[6] or phased arrays [7], [8]. In the former case, mechanical movement of a transducer is required, along one or two directions, to synthesize an aperture, which slows the acquisition process. In the latter one, dense all-electronic arrays are used which usually employ a large number of antenna elements and extra circuits (i.e. phase sifters) leading to complex and costly systems. The above limitations become more severe in higher frequencies, considering that Nyquist criterion usually need to be met to reassure enough resolution and low distortion in the final images.

DMAs typically consist of a waveguide with voltage-controlled metamaterial elements etched on its front surface [9]–[16]. A set of spatially distinct radiation patterns is generated at each control level by tuning the elements *on* and *off* [9]–[17]. The patterns are then emitted into the investigation domain simultaneously. Consequently, there is no need of mechanical moving parts or extra circuits for the pattern synthesis, leading to less power hungry and more cost-effective systems.

For imaging more complicated targets, multiple transmit (Tx) and receive (Rx) panels can be used in the form of multiple-input multiple-output (MIMO) systems [18]–[21]. A system like this is introduced in [14], [16]. Having multiple Txs, one way to transmit the signals to the investigation domain is to establish a time-division-based switching method where each Tx starts the transmission after the previous one finishes. The time needed to switch from one Rx-Tx combination to the next one, and repeat the transmission/reception for each one of them, is not negligible in the whole acquisition process, especially for a MIMO system consisting of multiple panels. In addition, the switching mechanism increases the power consumption and, hence, the cost, and, more significantly, adds insertion loss to the signal. To achieve the fastest possible acquisition time and avoid possible signal attenuation, in this work simultaneous transmission / reception from all Tx / Rx panels is considered. This is achieved by introducing orthogonal codes together with the transmitting waveform [22] so that the Tx signals can be separable at each receiver.

Once the back-scattered signal is captured at each receiver, an estimation of the imaged target can be obtained through a variety of reconstruction algorithms. Among these, algorithms in spatial domain, such as the single-shot matched filtering (MF) or the iterative least-squares (LS), have been shown to be very effective when imaging with DMAs [10]–[12], [23]–[28]. However, both depend on the calculation and then inversion of the aperture transfer function, also known as sensing matrix, which is a computationally expensive procedure [24]. In this work, image reconstruction is fully carried out in the frequency domain using a decompression step [13]–[17], [29] and the popular range migration algorithm (RMA) [9]. By avoiding the calculation and inversion of the sensing matrix, both the

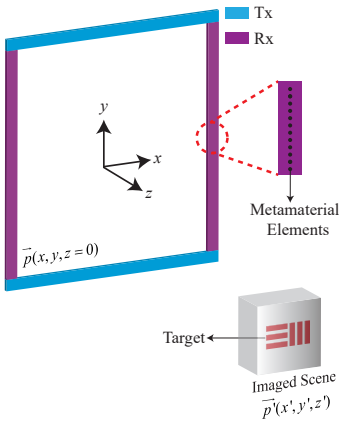

Fig. 1. The proposed DMA-based MIMO imaging configuration.

required hardware resources and the execution time of the algorithm can be significantly reduced [13]–[16].

In this paper, simulation results of the resolution target are presented to verify the suggested method. The rest of the paper is organized as follows: Section II introduces the model for coding the Tx signals, as well as the image reconstruction technique in the frequency domain. Section III presents and discusses the simulation results. Finally, Section IV summarizes the conclusions.

II. Orthogonal Coding Imaging With a MIMO DMA-based system

A. Channel coding and concurrent transmission

In this paper, we are considering a MIMO system as the one shown in Fig. 1, which consists of four DMA panels, two transmitting and two receiving. The elements of a DMA panel (i.e. metamaterial elements or metaelements) can be switched *on* and *off* using an external voltage stimulus, so that, for each control level, a part of them will radiate. This creates a set of spatially-diverse radiation patterns as a function of varying element configurations [9]–[16]. In this context, each of the *on/off* element distributions across the DMA constitutes a mask. Consequently, by cycling through the set of masks, a sequence of spatially distinct radiation patterns is generated from all Tx panels that illuminate the scene simultaneously. Similarly, the Rx panels utilize a sequence of masks to encode the back-scattered signal and compress it into one channel. The number of masks for the Tx and Rx panels is indicated by M_T and M_R, respectively.

Given this system, the goal is to obtain an estimate of the reflectivety of the scene σ, in the frequency domain, when all DMA panels are active *simultaneously*. To achieve this, transmitting signals need to be separable at each receiver and the technique adopted here is based on introducing orthogonal codes along the transmitting waveforms [22], [30].

The transmitting signal is modulated using a binary phase-shift keying (BPSK) scheme and the codes are are the columns of a matrix $\boldsymbol{W}_{C\times N_{Tx}}$, where C denotes the code length and N_{Tx} is the number of transmitters, in this case equal to two. The number of receivers is similarly denoted by N_{Rx}. The length of the code is subject to the condition $C > N_{Tx}$ [22], [30]. Considering the binary nature of the modulation each code is represented: $w_{c,t} \in \{-1, 1\}$, where $t = 1, 2, ...N_{Tx}$, such that the modulated transmitting signal generated for each mask is written:

$$h_t(a) = \mathrm{Re}\{\sum_{c=1}^{C} w_{c,t} P_A(a - cA) e^{+j\omega a}\}, \tag{1}$$

where a symbolizes the time, Re refers to the real part of the computed quantity, ω is the angular frequency, and P_A represents a rectangular pulse function with duration A.

The received signal is then written as:

$$d_r(a) = \sum_{t=1}^{N_{Tx}} Re\{G_{t,r}(m_T, m_R, f) \sum_{c=1}^{C} w_{c,t} P_A(a-cA) e^{+j\omega a}\} + n_r(a), \tag{2}$$

where $r = 1, 2, ..., N_{Rx}$, $G_{t,r}(m_T, m_R, f)$ denotes the frequency response involving the t-th Tx, r-th Rx, each frequency point and each Tx, Rx mask, where $m_T, m_R = 1, 2, ..., M_R$. More details about the computation can be found in [14], [16], [22], [30]. The term $n_r(t)$ refers to the measurements noise, which is ignored in this paper.

After down-conversion and sampling the received signal is written as follows:

$$d_r[c] = \sum_{t=1}^{N_{Tx}} G_{t,r}(m_T, m_R, f) w_{c,t} + b_r + n_r[c], \tag{3}$$

where b_r represents a DC offset of the down-converter, a phenomenon also ignored in this paper. After concatenating the C samples we can write:

$$\boldsymbol{d}_r = \boldsymbol{W}\boldsymbol{G}_{t,r}, \tag{4}$$

Taking under consideration that the Tx codes are selected such that they are orthogonal, such that $W^\dagger W = LI$, where $W^\dagger$ is the conjugate transpose of W, and I denotes the identity matrix, we can multiply both sides of (4) with $W^\dagger$ and get:

$$\boldsymbol{g}_{t,r} = \frac{1}{C}\boldsymbol{W}^\dagger \boldsymbol{d}_r. \tag{5}$$

Eq. (5) suggests that for each Rx panel the signals coming from Tx panels are separated ($\boldsymbol{g}$ is written in terms of t and r).

B. Image reconstruction in the frequency domain

Reconstruction of images in the frequency domain, using the conventional RMA algorithm [1], becomes more challenging when compressive antennas such as the DMAs in Fig. 1 are used. That is because, unlike the conventional SAR or phased arrays imaging, where a uniform grid of measurements is present, the signal is compressed at the receiver panel through the aperture's transfer function (i.e., the sensing matrix). However, recent literature has shown that if the aperture fields are known, through a near-field scan, it is possible to decompress

the signal as if it had been acquired from a set of independent dipoles along the DMA panel [13]–[17], [29].

In [14], [16] we presented the mathematical derivation of the uniform signal in the case where a square DMA unit is used, identical to the one illustrated in Fig. 1. The algorithm is then called MD-RMA (MIMO DMA-RMA). In summary, if the fields of Tx and Rx panels are known and stored in matrices $\mathbf{\Phi}_t$ and $\mathbf{\Phi}_r$ respectively, the decompression step is written as follows:

$$S(x_i,t,y_l,r,f) = \sum_{m_T=1}^{M_T}\sum_{m_R=1}^{M_R} \Phi^{+}_{t,m_T}(x_i,f) g_{m_T,m_R}(t,r,f) \Phi^{+}_{r,m_R}(y_l,f), \quad (6)$$

where x_i and y_l are the positions of the metamaterial elements along the Tx and Rx panels respectively, $i = 1,...,N_T$ and $l = 1,...,N_R$, and N_T, N_R is the total number of elements on each Tx, Rx panel, respectively. In this case, $N_T = N_R$. The above equation can be written in matrix form as:

$$\boldsymbol{S}(t,r,f) = \mathbf{\Phi}^{+}_t(f) g(t,r,f) \mathbf{\Phi}^{T^+}_r(f), \quad (7)$$

where ^{T} symbolizes the transpose of a matrix. After this step, the signal S is finally in the form of a conventional MIMO signal, i.e., in terms of each transmitting and receiving position, and, for better visualization, it can be written as $S(x_T, y_T, x_R, y_R, f)$.

An important note for the decompression is that the $\mathbf{\Phi}$ matrix depends on the properties of each DMA (e.g. set of masks), and it is extracted for each individual DMA. Therefore, the transformation of (7) should be done for each Tx-Rx combination. Applying the channel coding technique presented in the previous section, it is possible to separate the Tx signals on each receiver. However, it is not possible for each receiver to know from which particular transmitter each signal is emitted. To hold the proposed decompression step, we need to assume that the Tx panels have identical $\mathbf{\Phi}$ matrices. This condition, in practice, can be realized by using the same types of DMAs as the Tx antennas choice. Alternatively, an MF or LS algorithm can be used, which does not require this distinction. However, this alternative brings the computational limitations discussed earlier in the Introduction section.

After the signal is written in the form $S(x_T, y_T, x_R, y_R, f)$ following the decompression step, it can be effectively reconstructed using the range migration techniques available for MIMO systems [18], [19], [21]. First, a multistatic-to-monostatic (MTM) conversion step is applied to transform the signal in a monostatic-like form:

$$\hat{S}(x_c,y_c,f) = S(x_T,y_T,x_R,y_R,f)\frac{\hat{s}_{\text{ref}}(x_c,y_c,f)}{s_{\text{ref}}(x_T,y_T,x_R,y_R,f)}, \quad (8)$$

where $\hat{s}_{\text{ref}}$ and s_{ref} are the reference signals and (x_c, y_c) are the coordinates of the monostatic virtual grid. More details for their calculation can be found in [18], [19], [21].

Then, the conventional RMA can be used to retrieve an estimate $\hat{\sigma}$ of the investigation scene:

$$\hat{\sigma}(x',y',z') = \text{IFFT}_{3D}[Stolt[\text{FFT}_{2D}[\hat{S}(x_c,y_c,f)]e^{-j\sqrt{4k^2-k_x^2-k_y^2}z_0}]], \quad (9)$$

where FFT and IFFT denote the forward and inverse fast Fourier transform respectively. The exponential term refers to the dispersion relationship for monostatic apertures [1], k_x, k_y, k represent the wavenumber vectors, and z_0 is the distance to the center of the investigation domain. The Stolt interpolation refers to the 1D interpolation step which is essential to remap the data corresponding to the non-uniform k_z domain resulting from the non-linear dispersion relationship to a uniform one, so that the 3D IFFT can be applied.

III. Simulation Results

In this section, we provide simulation results using resolution targets when the channel coding technique along with the MD-RMA algorithm presented in the previous section is used. The results are shown in comparison with the case where non concurrent transmission/reception is occurring and, therefore, we are switching between Tx and Rx channels (DMA panels) each time.

For the numerical results, the MIMO system shown in Fig. 1 is considered. The panel size is equal to $D = 35$ cm and $N_T = N_R = 26$ metaelements are placed alongside its length separated by $\lambda_{\text{min}}/2$, where λ_{min} is the wavelength at the maximum frequency. The number of masks is equal to $M_T = M_R = 40$. For each mask, half of the elements are radiating and the rest are considered to be switched *off*. The frequency band ranges from 17.5 GHz to 22 GHz equally sampled at $N_F = 41$ frequency steps. Therefore, the number of measurement modes for this system is equal to $N_{T_x} \times N_{R_x} \times M_T \times M_R \times N_F = 262400$. Finally, the investigation domain is the volume between $x' \in [-0.18, 0.18]$ m, $y' \in [-0.18, 0.18]$ m, $z' \in [0.9, 1.1]$ m. The distance from the synthesized aperture to the center of the imaging scene is $z_0 = 1.0$ m along the z direction.

For the orthogonal coding scheme, a BPSK modulation is considered as mentioned in the previous section; therefore, the code symbols are binary in the set $W_{l,t} \in \{-1, 1\}$, and more specifically, each code sequence forms a column of a Hadamard matrix [31]. The code length is equal to $L = 4$ for this paper, such that the codes matrix W is of size $\boldsymbol{W}_{4\times 2}$.

Taking into account the above parameters, the cross-range ($xy-$plane) and range ($zy-$plane) resolution limits are calculated approximately equal to $\delta_{cr} = \lambda_{\text{min}} z_0/2D = 20$ mm and $\delta_r = c/2B = 33$ mm, respectively. The resolution target is constructed of horizontal and vertical stripes that are separated by δ_{cr}. The width of the stripes is also selected to be δ_{cr}. A depiction of the imaged resolution target is shown in Fig. 2(a). The reconstructed image of the resolution target when time-based channel switching occurs between each transmission / reception is shown in Fig. 2(b). The reconstruction of the same resolution target when orthogonal channel coding is used to

TABLE I
THE EXECUTION TIME FOR EACH STEP OF RECONSTRUCTION PROCEDURE (IN SECONDS)

Switching	Separating Signal	MD-RMA	Total
No	0.19	2.68	2.86

allow concurrent transmission/reception is shown in Fig. 2(c). Fig. 2 illustrates a qualitative comparison between resolution targets for the both cases, showing that we can have the same quality of reconstruction when all DMA panels are active at the same time, eliminating the time and hardware needed for switching the channels to separate the Tx, Rx combinations. The actual normalized means square error (NMSE) between Fig. 2(b) and Fig. 2(c) is of the order 0.001.

Regarding execution time, in the case of channel coding, we should also consider the step needed to separate the Tx signals at each receiver. After this step, the image is fully reconstructed by the MD-RMA algorithm [14], [16]. Indicatively, the execution time (in seconds) for these steps is shown in Table I. These times refer only to central processing unit (CPU) execution, using MATLAB 2021b on a computer with 64-bit Windows 10 operating system, 16 GB of random access memory (RAM), and a Core i7-8700 CPU, and they are the average time of ten consecutive executions.

An objective comparison with the time-division-based switching case in terms of data acquisition time, cannot be straightforward because it depends on the switching method (i.e. electromechanical, all-electronic) and the design of the particular Tx and Rx panels. An electronic switch needs only a few milliseconds (ms) to switch between two states. Therefore, in the case of such a small system as the one of Fig. 1, also accounting for the time needed to separate the signals on each receiver, the benefit from the concurrent transmission/reception may not be that apparent in the acquisition process time. However, scaling this system to a larger one, consisting of multiple panels, multiple switches are needed to cover all Tx-Rx combinations, and additionally, more time is needed to transmit/receive for each one of the Tx-Rx pairs. Furthermore, eliminating the insertion loss inherent to all switching methods and simplifying the hardware, and, hence, the cost of the system, constitute significant advantages of the suggested method that are evident even in small scale systems such as the one discussed in this paper.

IV. CONCLUSION

In this paper, we proposed an orthogonal channel coding technique for a MIMO DMA-based system. Following the presented approach, we can benefit from transmitting and receiving from all DMA panels simultaneously, while the Tx contributions are still separable on each receiver. Consequently, since the received signals can be written in terms of Rx, Tx contributions, a frequency domain algorithm, called MD-RMA, was used to reconstruct the image. Evaluating the results presented in this work, the quality of the reconstructed images using the proposed layout and the MD-RMA algorithm are not affected by the channel coding step. Furthermore, separating the signals at each receiver adds negligible time to the reconstruction process.

ACKNOWLEDGMENT

This work was supported by the Leverhulme Trust under the Research Leadership Award RL-2019-019. The work of María García-Fernández and Guillermo Álvarez-Narciandi was supported by the UKRI Postdoctoral Fellowship Guarantee for Marie Skłodowska-Curie Action Postdoctoral Fellowships under Projects EP/X022951/1 and EP/X022943/1.

REFERENCES

[1] D. M. Sheen, D. L. McMakin, and T. E. Hall, "Three-dimensional millimeter-wave imaging for concealed weapon detection," *IEEE Transactions on microwave theory and techniques*, vol. 49, no. 9, pp. 1581–1592, 2001.

[2] Y. Wang and A. E. Fathy, "Advanced system level simulation platform for three-dimensional uwb through-wall imaging sar using time-domain approach," *IEEE Transactions on Geoscience and Remote Sensing*, vol. 50, no. 5, pp. 1986–2000, 2011.

[3] M. Elsdon, O. Yurduseven, and D. Smith, "Early stage breast cancer detection using indirect microwave holography," *Progress In Electromagnetics Research*, vol. 143, pp. 405–419, 2013.

[4] A. Moreira, P. Prats-Iraola, M. Younis, G. Krieger, I. Hajnsek, and K. P. Papathanassiou, "A tutorial on synthetic aperture radar," *IEEE Geoscience and remote sensing magazine*, vol. 1, no. 1, pp. 6–43, 2013.

[5] A. W. Doerry and F. M. Dickey, "Synthetic aperture radar," *Optics and photonics news*, vol. 15, no. 11, pp. 28–33, 2004.

[6] M. Fallahpour, J. T. Case, M. T. Ghasr, and R. Zoughi, "Piecewise and wiener filter-based sar techniques for monostatic microwave imaging of layered structures," *IEEE Transactions on Antennas and Propagation*, vol. 62, no. 1, pp. 282–294, 2013.

[7] S. Withington, G. Saklatvala, and M. P. Hobson, "Partially coherent analysis of imaging and interferometric phased arrays: noise, correlations, and fluctuations," *JOSA A*, vol. 23, no. 6, pp. 1340–1348, 2006.

[8] A. J. Fenn, D. H. Temme, W. P. Delaney, and W. E. Courtney, "The development of phased-array radar technology," *Lincoln Laboratory Journal*, vol. 12, no. 2, pp. 321–340, 2000.

[9] D. R. Smith, O. Yurduseven, L. P. Mancera, P. Bowen, and N. B. Kundtz, "Analysis of a waveguide-fed metasurface antenna," *Physical Review Applied*, vol. 8, no. 5, p. 054048, 2017.

[10] T. Sleasman, M. Boyarsky, M. F. Imani, J. N. Gollub, and D. R. Smith, "Design considerations for a dynamic metamaterial aperture for computational imaging at microwave frequencies," *JOSA B*, vol. 33, no. 6, pp. 1098–1111, 2016.

[11] T. Sleasman, M. F. Imani, J. N. Gollub, and D. R. Smith, "Dynamic metamaterial aperture for microwave imaging," *Applied Physics Letters*, vol. 107, no. 20, p. 204104, 2015.

[12] T. Sleasman, M. Boyarsky, M. F. Imani, T. Fromenteze, J. N. Gollub, and D. R. Smith, "Single-frequency microwave imaging with dynamic metasurface apertures," *JOSA B*, vol. 34, no. 8, pp. 1713–1726, 2017.

[13] L. Pulido-Mancera, T. Fromenteze, T. Sleasman, M. Boyarsky, M. F. Imani, M. Reynolds, and D. Smith, "Application of range migration algorithms to imaging with a dynamic metasurface antenna," *JOSA B*, vol. 33, no. 10, pp. 2082–2092, 2016.

[14] V. Skouroliakou, A. M. Molaei, M. García-Fernández, G. Álvarez-Narciandi, and O. Yurduseven, "Frequency domain image reconstruction for imaging with multistatic dynamic metasurface antennas," *IEEE Access*, vol. 10, pp. 124 728–124 737, 2022.

[15] V. Skouroliakou, A. M. Molaei, and O. Yurduseven, "Towards real-time three-dimensional (3d) imaging using dynamic metasurface antennas," in *2023 17th European Conference on Antennas and Propagation (EuCAP)*. IEEE, 2023, pp. 1–5.

[16] V. Skouroliakou, A. M. Molaei, M. Garcia-Fernandez, G. Alvarez-Narciandi, and O. Yurduseven, "Range migration algorithm for a multistatic 3d compressive computational imaging system with dynamic metasurface aperture," in *2023 24th International Radar Symposium (IRS)*. IEEE, 2023, pp. 1–10.

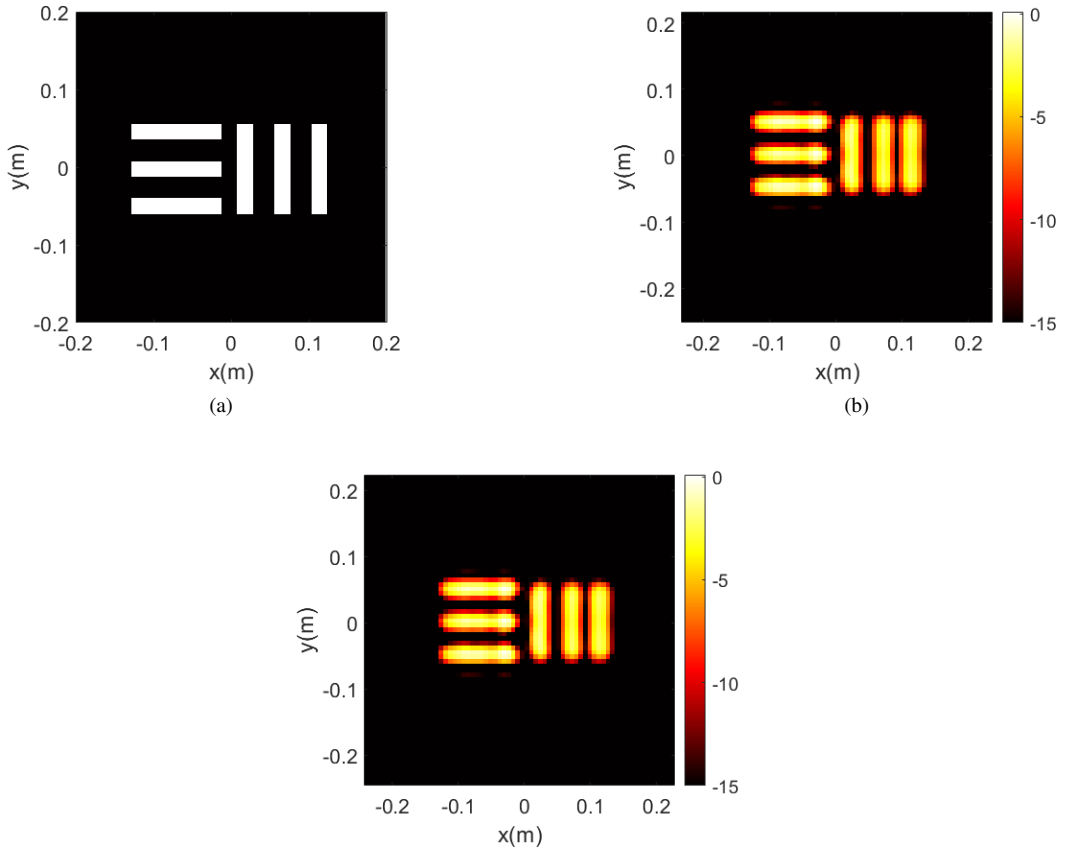

Fig. 2. The resolution target and reconstructed images with MD-RMA algorithm: (a): Actual target image, (b): reconstructed image when switching between channels, and (c): reconstructed image when concurrent transmission is occurring.

[17] A. V. Diebold, L. Pulido-Mancera, T. Sleasman, M. Boyarsky, M. F. Imani, and D. R. Smith, "Generalized range migration algorithm for synthetic aperture radar image reconstruction of metasurface antenna measurements," *JOSA B*, vol. 34, no. 12, pp. 2610–2623, 2017.

[18] W. F. Moulder, J. D. Krieger, J. J. Majewski, C. M. Coldwell, H. T. Nguyen, D. T. Maurais-Galejs, T. L. Anderson, P. Dufilie, and J. S. Herd, "Development of a high-throughput microwave imaging system for concealed weapons detection," in *2016 IEEE International Symposium on Phased Array Systems and Technology (PAST)*. IEEE, 2016, pp. 1–6.

[19] Z. Wang, Q. Guo, X. Tian, T. Chang, and H.-L. Cui, "Near-field 3-d millimeter-wave imaging using mimo rma with range compensation," *IEEE Transactions On Microwave Theory and Techniques*, vol. 67, no. 3, pp. 1157–1166, 2018.

[20] T. Fromenteze, O. Yurduseven, F. Berland, C. Decroze, D. R. Smith, and A. G. Yarovoy, "A transverse spectrum deconvolution technique for mimo short-range fourier imaging," *IEEE Transactions on Geoscience and Remote Sensing*, vol. 57, no. 9, pp. 6311–6324, 2019.

[21] V. Skouroliakou, A. M. Molaei, V. Fusco, and O. Yurduseven, "Fourier-based radar processing for multistatic millimetre-wave imaging with sparse apertures," in *European Conference on Antennas and Propagation*, 2021.

[22] A. Pedross-Engel, D. Arnitz, J. N. Gollub, O. Yurduseven, K. P. Trofatter, M. F. Imani, T. Sleasman, M. Boyarsky, X. Fu, D. L. Marks *et al.*, "Orthogonal coded active illumination for millimeter wave, massive-mimo computational imaging with metasurface antennas," *IEEE Transactions on Computational Imaging*, vol. 4, no. 2, pp. 184–193, 2018.

[23] O. Yurduseven, M. F. Imani, H. Odabasi, J. Gollub, G. Lipworth, A. Rose, and D. R. Smith, "Resolution of the frequency diverse metamaterial aperture imager," *Progress In Electromagnetics Research*, vol. 150, pp. 97–107, 2015.

[24] O. Yurduseven, J. N. Gollub, A. Rose, D. L. Marks, and D. R. Smith, "Design and simulation of a frequency-diverse aperture for imaging of human-scale targets," *IEEE Access*, vol. 4, pp. 5436–5451, 2016.

[25] O. Yurduseven, M. A. B. Abbasi, T. Fromenteze, and V. Fusco, "Lens-loaded coded aperture with increased information capacity for computational microwave imaging," *Remote Sensing*, vol. 12, no. 9, p. 1531, 2020.

[26] T. Fromenteze, O. Yurduseven, P. Del Hougne, and D. R. Smith, "Lowering latency and processing burden in computational imaging through dimensionality reduction of the sensing matrix," *Scientific reports*, vol. 11, no. 1, pp. 1–14, 2021.

[27] J. Hunt, T. Driscoll, A. Mrozack, G. Lipworth, M. Reynolds, D. Brady, and D. R. Smith, "Metamaterial apertures for computational imaging," *Science*, vol. 339, no. 6117, pp. 310–313, 2013.

[28] T. V. Hoang, V. Fusco, T. Fromenteze, and O. Yurduseven, "Computational polarimetric imaging using two-dimensional dynamic metasurface apertures," *IEEE Open Journal of Antennas and Propagation*, vol. 2, pp. 488–497, 2021.

[29] A. M. Molaei, V. Skouroliakou, V. Fusco, and O. Yurduseven, "Efficient 3d image reconstruction for near-field microwave imaging using dynamic metasurface antenna," *IEEE Access*, vol. 10, pp. 68 491–68 498, 2022.

[30] A. M. Molaei, S. Hu, R. Kumar, and O. Yurduseven, "Mimo coded generalized reduced dimension fourier algorithm for 3-d microwave imaging," *IEEE Transactions on Geoscience and Remote Sensing*, vol. 61, pp. 1–15, 2023.

[31] K. J. Horadam, *Hadamard matrices and their applications*. Princeton university press, 2012.